



## City Research Online

### City, University of London Institutional Repository

---

**Citation:** Bruecker, C., Wagner, R. & Koehler, M. (2016). Measurements of wall-shear stress fields on the piston crown in an IC engine flow using fluorescent labelled micro-pillar imaging. Paper presented at the 18th International Symposium on Applications of Laser Techniques to Fluid Mechanics, 4-7 Jul 2016, Lisbon, Portugal.

This is the accepted version of the paper.

This version of the publication may differ from the final published version.

---

**Permanent repository link:** <https://openaccess.city.ac.uk/id/eprint/21325/>

**Link to published version:**

**Copyright:** City Research Online aims to make research outputs of City, University of London available to a wider audience. Copyright and Moral Rights remain with the author(s) and/or copyright holders. URLs from City Research Online may be freely distributed and linked to.

**Reuse:** Copies of full items can be used for personal research or study, educational, or not-for-profit purposes without prior permission or charge. Provided that the authors, title and full bibliographic details are credited, a hyperlink and/or URL is given for the original metadata page and the content is not changed in any way.

---

City Research Online:

<http://openaccess.city.ac.uk/>

[publications@city.ac.uk](mailto:publications@city.ac.uk)

---

# Measurements of wall-shear stress fields on the piston crown in an IC engine flow using fluorescent labelled micro-pillar imaging

C. Brücker<sup>1,\*</sup>, R. Wagner<sup>2</sup>, M. Köhler<sup>2</sup>,

1: Dept. of Aeronautical Engineering, City University London, United Kingdom

2: Dept. of Fluid Mechanics, TU Bergakademie Freiberg, Germany

\* Correspondent author: christoph.bruecker@city.ac.uk

**Keywords:** IC engine flow, micro-pillar imaging, wall-shear stress, fluorescent labelled, optical wave guide

## ABSTRACT

The measurement of wall shear-stress along the crown of a moving piston is accomplished with an array of hair-like, flexible micro-pillar sensors (MPS) in an internal combustion (IC) engine during intake flow conditions. The MPS are wall-clamped flexible micro-cylinders of 20micron diameter made of polydimethylsiloxane (PDMS) positioned on the surface of a transparent planar piston crown and protruding into the boundary layer flow above the piston at a height of 390micron. Their tips are labelled with fluorophores and are illuminated with a scanning laser-sheet system that follows the piston motion in synchronous manner. The flow-induced deflection is recorded through the transparent piston crown from below with a compact shaft-mounted high-speed camera recording the fluorescent re-emitted light from the pillar tips and using the fact of optical wave-guide features of the transparent micro-pillars. The experiments were performed in a transparent 4-valve engine setup (1.6 liter Prince 2, N13B16) during the intake phase. In order to improve the temporal resolution, the running speed of the engine was scaled down using water as working liquid. A static and dynamic sensor-calibration enabled the precise measurements of the wall-shear stress distribution with the sensor array. Due to spatial resolution limits of current available compact high-speed camera the recorded region along the piston was limited to 4x2 mm<sup>2</sup> with 8x4 pillars in full view. The recordings at 300fps show the WSS fluctuations induced by the valve-jet / piston-wall interaction in the beginning of the intake with strong wall-normal motion forming critical points in the WSS field such as saddles, nodes and foci. Over the intake cycle > CA 80° these fluctuations die out and flow is transformed into wall-parallel coherent motion prescribed by the formation of the tumble.

---

## 1. Introduction

The in-cylinder flow mixing and combustion processes strongly depend on the flow interaction and heat transfer with the inner walls, i.e. the cylinder head, the cylinder walls and the piston crown. Formation of hydrocarbons, carbon monoxide and soot is highly influenced by these near-wall boundary layer flows. The trend towards decreasing fuel consumption at increasing power output is pushing the industry to “downsized” engines with smaller bore. This goes with an increasing ratio of total surface area to combustion chamber volume which further increases

the relevance of the near-wall processes for efficient generation of required power density. The ability to measure the flow field in IC engines close to the wall of the piston is of particular interest to understand the appearance of hot-spots or weak wash-out. This requires developing new measurement technologies that are able to record the wall shear stress distribution and temperature field close at these moving walls in time over the whole cycle.

Such a new technology is presented herein which uses a scanning light-sheet and a co-moving compact high-speed camera integrated within the piston shaft, both synchronized with the piston motion. The nowadays super-compact sizes of high-resolution CMOS cameras allowed integrating such a camera in the piston shaft. Typically, these cameras are also useful for Time-Resolved PIV (TR-PIV) systems which made large progress towards successful application in IC engine flows in the recent years. Borée & Miles (2014) investigated the spatial structure of the flow and its temporal evolution during a series of consecutive cycles via TR-PIV in a research engine of moderate tumbling ratio. They also studied the flow details during the intake cycle to understand the cause of cycle-to-cycle fluctuations in the intake phase. However, it is only recently that first near-wall PIV measurements could be realized within transparent engines. A flying PIV system was developed by Köhler et al. (2015) which is able to measure the boundary layer development above the piston crown while the piston is moving. This offered to the first time time-resolved recordings of wall-parallel motion in a radial plane 1.5mm above the piston at the edge of the boundary layer. However, so far these flying PIV measurements were not sufficiently close to the wall to resolve the wall-shear stress.

The system developed in our lab is based on the same technology using a compact, piston-shaft mounted camera technology in combination with a motion-synchronized scanning light-sheet. With implementation of the method of micro-pillar wall-shear stress imaging (Brücker et al. 2005) this allows us to investigate the evolution of the near-piston flow topology and to distinguish regions of high wall-shear or flow separation due to the interaction of vortices or the tumble flow with the piston wall. The scanning light-sheet herein does not illuminate any tracer-particles added to the flow but the fluorescent marked tips of flexible micro-pillar wall shear sensors at the surface of the piston crown. The co-moving compact high-speed camera below the piston then records the scattered light from the bended tips and image processing is used to determine the displacement of the tip relative to their position at rest. This measure can be related to the local WSS as described in the original publication by Brücker et al. (2005). The bending of the flexible hair-like structures is recorded in submicron resolution and can be related

to the local wall shear-stress after calibration. The schematic concept is given in Figure 1 to illustrate the implementation of the principle to an internal flow of a 4-valve engine in the intake phase.

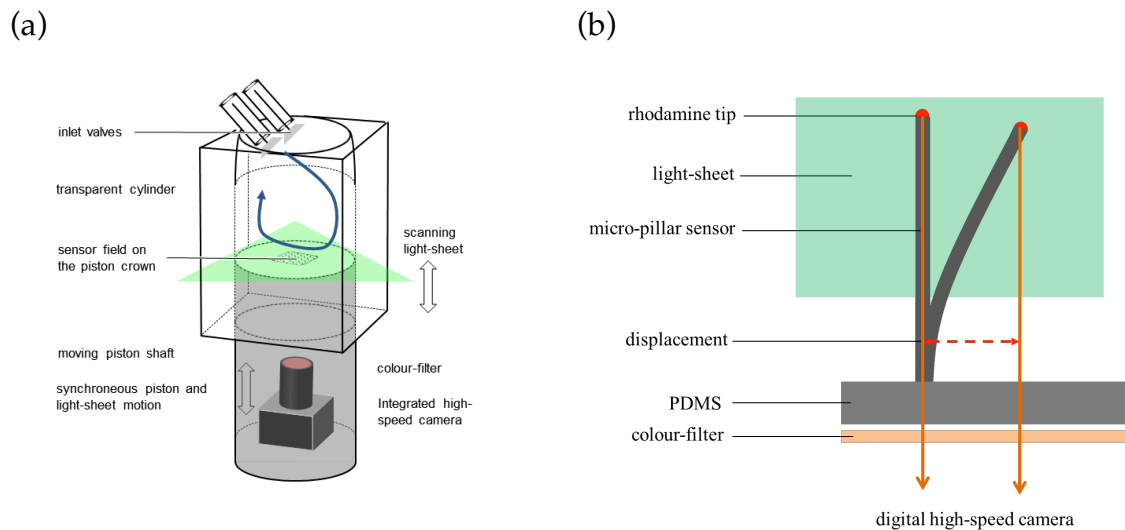


**Fig 1.** Principle for the optical acquisition of the micro-pillar deflection from below through the transparent piston crown (a) and zoomed sketch that shows one single pillar in the sensor array (b). The tips of the micro-pillars are labelled with fluorophores (red rhodamine dot on the pillar tips) which are excited by a Nd:YLF laser that is expanded to a light-sheet (green bar) and follows the moving piston crown in synchronous manner. The re-emitted light of the tips is recorded by a shaft-mounted camera below the piston that receives the light through the transparent pillar and piston, while the direct laser light is blocked with a color filter.

## 2. Experimental setup and methods

### *The model engine*

The experiments were carried out in a transparent version of an original 4-valve cylinder head with a displacement of 1.6 liters (BMW Prince 2), see figure 2 and compare also Koehler et al. (2015). The working fluid is water. Table 1 shows the characteristic dimensions of the engine. The piston and the valves are driven by synchronized single linear traverse motors (Mannesmann MDD065). To accomplish full optical access, the original cylinder and piston is replaced by a transparent version made of perspex. The linear motors can follow different path-time diagrams which allow an easy change of the valve timings. The maximum valve stroke is 9 mm. For the present investigations the piston is moved in vertical direction in the time-profile

of a sine path. While the downward movement, the piston aspirates water from a reservoir. After 180° CAD in BDC-position the exhaust valves open and the piston starts pushing the liquid back into the reservoir. The water in the reservoir can be heated up to temperatures of 80°C to reduce the viscosity and increase the Reynolds-number, thus representing higher running speeds within the original engine. For the described investigations, the water was heated up to 50°C. All measurements within the water analogue refer to typical engine speeds of 950 U/min.

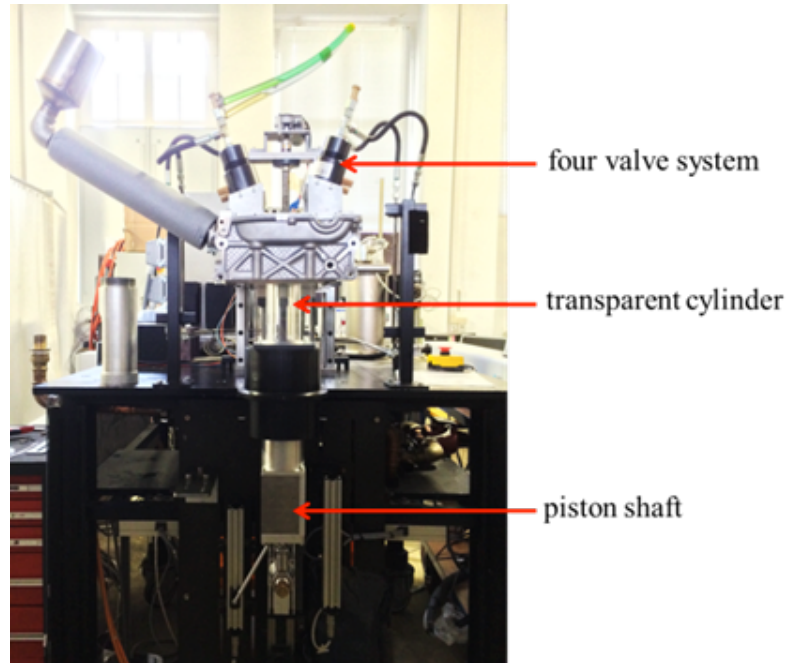
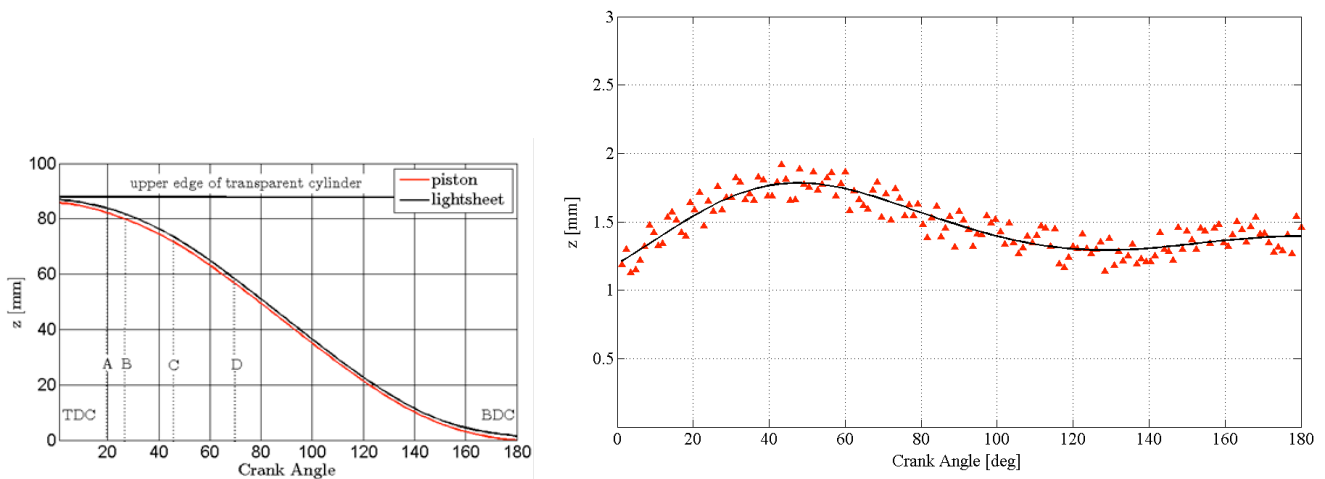


Fig 2: Picture of the 4-valve IC engine with transparent cylinder and motor-driven piston

Bore $b$	76,5 mm	working fluid	water
Stroke $S$	85,8 mm	temperature	50 °C
valve stroke	9 mm	density	$0,98 \times 10^3 \text{ kg/m}^3$
Clearance	6 mm	kinematic viscosity	$0,55 \times 10^{-6} \text{ m}^2/\text{s}$
$U_{\text{max piston}}$	0,15 m/s	Re	$\approx 21000$
$N_{\text{real}}$	950 rpm	real fluid	air

Table 1: Engine setup and fluid characteristics



**Fig. 3** Left: motion profile of the piston crown (black line) and the position of the light-sheet at maximum intensity. right: enlarged view of the jitter in vertical light-sheet offset relative to the piston crown

The profiles in Fig. 3 display the vertical position of the moving light sheet and the piston head during the intake cycle. Therefore black paper was wrapped around the piston crown and the reflections mark the light-sheet position. The light-sheet is generated with a pulsed Nd:YLF laser (Litron Nd:YLF, 30 mJ at 300 Hz repetition rate, wavelength 527 nm) and equipped with a light-sheet optic in front of the light arm. Both the reference edge of the piston head and the light sheet position are captured during the motion cycle with an external high-speed camera looking from the side. As seen from the profiles, the light-sheet remains in nearly constant distance relative to the piston with an average distance of 1.5 mm. Deviations from the average are less than 0.4 mm within the complete cycle and they are maximum only near to the begin (TDC) and end (BDC) of the intake cycle. For the present measurement, the thickness of the light-sheet was adjusted to a  $e^{-2}$  thickness of  $w \approx 3$  mm to ensure that the tips of the pillars are always illuminated.

### *Micro-pillar imaging*

Our studies focus on a region located around the center of the piston. A quadratic PDMS sheet (Poly-Dimethylsiloxane,  $\rho = 1050$  kg/m<sup>3</sup>, Young's modulus  $E \approx 1.76 \times 10^6$  N/m<sup>2</sup>) with a 2D array of 30×30 flexible filaments on its surface was placed at the center in a cavity inside the perspex crown such that the sheet surface was flush with the planar crown's upper surface. The slender filament-like micro-pillars protruding out of the PDMS sheet have a diameter of  $D = 20 \mu\text{m}$  and a height of  $L = 390 \mu\text{m}$ . In rest conditions, the axes of the structures are oriented in wall-normal

direction. They form a regular array with a spacing of  $\Delta x, \Delta y = 500\mu\text{m}$ , see Fig 4. Other than in the previous documented applications of the technique, the herein used pillars were labelled on their tips with rhodamine dye. This fluorescent pigment emits the light in a different wavelength than the incident laser-light. with the result that only the light of the pillar tip passes through the colour-filter (orange filter) and reaches the camera chip (Blue-Cougar-XD104, 1024×499 px, 300fps) below the piston. Recordings were taken with a temporal resolution of 1.5 frames/CA. Within the viewing field of the camera a number of 8×4 pillars can be seen. Typically a total number of 270 frames were stored in the on-board memory of the camera during one run.

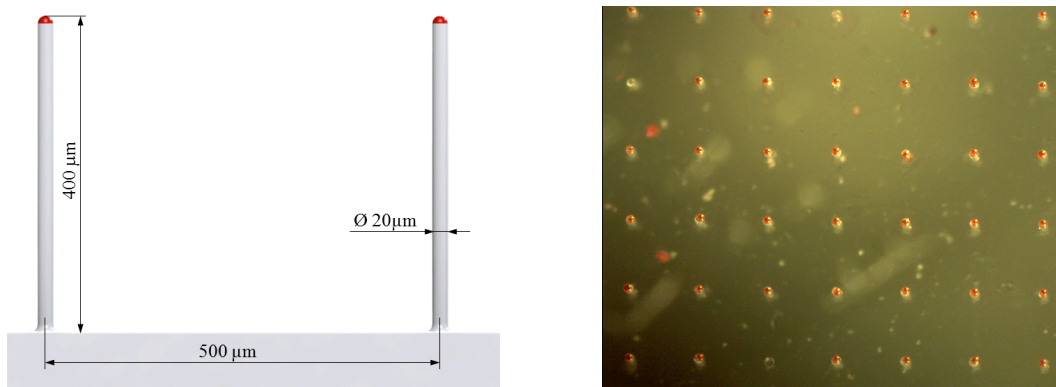


**Fig 4** Picture of the fluorescent labelled pillar tips (left) as seen from top onto the regular array mounted in the piston crown (right). Note that the tips increase the length of the pillars about 10micron.

The static and dynamic sensor response was investigated using the methods described in Skupsch et al (2012). The damped natural frequency of the micro-pillar in water is about  $f_{0,d} \approx 1053\text{Hz}$ . With  $f \leq 0,3 f_0$  the application range of the sensor array can be found at a frequency of approximately  $f \leq 250\text{Hz}$  with a response time of about 4ms, see Fig. 5. Note that the 2<sup>nd</sup> order mechanical system with a quality-factor of  $QF \approx 0.7$  is overdamped, thus no resonances appear and maximum bandwidth is achieved (Brücker et al. 2007). The two-dimensional wall shear stress vector is defined as

$$\tau_w = \rho v \left. \frac{\partial \mathbf{u}_\perp}{\partial z} \right|_{z=0} = f(\mathbf{Q}) \quad (1)$$

where the subscript  $\perp$  denotes the two horizontal (or tangential) x- and y-components of coordinates along the wall of the piston crown. Skin friction and wall stress fields are defined by velocity derivatives normal to the wall in z-direction. Measurements of the pillar tip deflection

with the camera looking from below the crown provide the projection of the end-to-end vector in the wall-parallel x-y-plane  $\mathbf{Q}$  with its components  $Q_x$  and  $Q_y$ . This describes the WSS vector in orientation and magnitude, see eq. (1). The functional relation is provided by the calibration procedure.

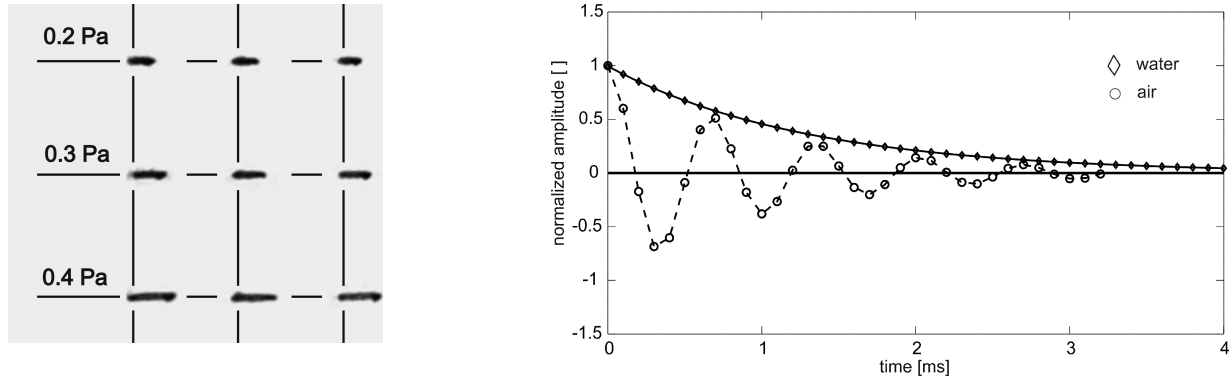


**Fig. 5** Left: top view images of a row of pillars in the Couette device for calibration purpose. A grid is overlaid to show the spacing of the pillars at rest. Note that the imaging in the calibration procedure is from top onto the pillar tips and different from the situation in the engine flow experiments. The calibration provides a square root behavior of  $\tau_w = -0.145 + \sqrt{0.021 + 0.715 w^*}$  [Pa] with  $w^* = w_{Tip} / L$ . right: pillar tip motion profile after enforced deflection and damped oscillation back to rest, recorded at 10kHz. The response time is about 4ms.

The calibration shows a sensitivity of about 23mPa/px which remains nearly constant up to frequencies of 100Hz and then starts to roll-off at -20db for higher frequencies.

A special concept of the proposed technology is the sub-surface imaging of the tip motion with use of the wave-guide properties of the micro-pillars, the latter being already pointed out in the original publication by Brücker et al (2005).

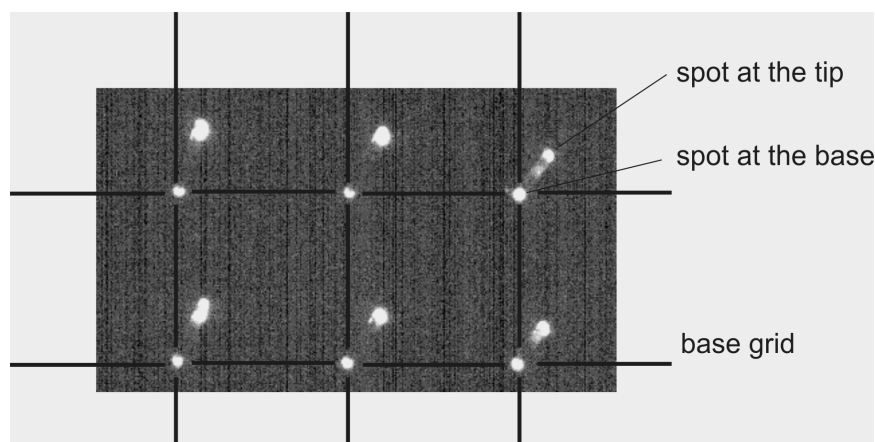


**Fig 6** Typical image of the fluorescent labeled micro-pillar tips from below the surface when looking through the transparent piston and PDMS layer onto the tips

A typical image after simple contrast-enhancement provides a characteristic pattern, which consists of the direct light spot received from the tip plus an additional spot that originates from the emitted light that is guided through the micro-pillar towards the footage and is then received by the camera, see Fig 6. This offers a direct measure of the components  $Q_x$  and  $Q_y$  as the shift between the tip spot and the base spot. The image processing routines achieve an accuracy of roughly 0.3 px in the centroid position which corresponds to a minimum resolved wall shear stress of about 10mPa. All images are processed and the detected shifts are being processed further on. One of the procedure is the determination of critical points (CPs) in the WSS field out of the spatio-temporal data field. Following the discussion in Brücker (2015) the local topology of CPs in WSS is given by the similarity invariant of the no-slip tensor  $A$  computed at the CP. Within a linear approximation in the vicinity of the CP the invariant simplifies to

$$p = \text{tr}(A) = \text{tr} \left( \begin{bmatrix} \partial^2 u / \partial x \partial z & \partial^2 u / \partial y \partial z \\ \partial^2 v / \partial x \partial z & \partial^2 v / \partial y \partial z \end{bmatrix} \right) \approx \text{tr} \left( \begin{bmatrix} \partial Q_x / \partial x & \partial Q_x / \partial y \\ \partial Q_y / \partial x & \partial Q_y / \partial y \end{bmatrix} \right) = \text{div}(\mathbf{Q}) \quad (2)$$

Therefore CPs can be found in our results where the divergence  $p = \nabla \cdot \mathbf{Q}$ , calculated from the  $\mathbf{Q}$ -vector field on the regular grid by central difference schemes, is large. A physical interpretation of a large  $p$ -value on the pillar field is a strong wall-normal fluid motion close to the wall which is generated by vortical structures interacting with the wall.

### 3. Results

The considered sensor field within the  $30 \times 30$  array is slightly offset with respect to the piston center, see Fig. 6. A series of original images with overlaid tip displacement vectors is given on the right-hand side. In the lower row of the picture the static reference markers can be seen.

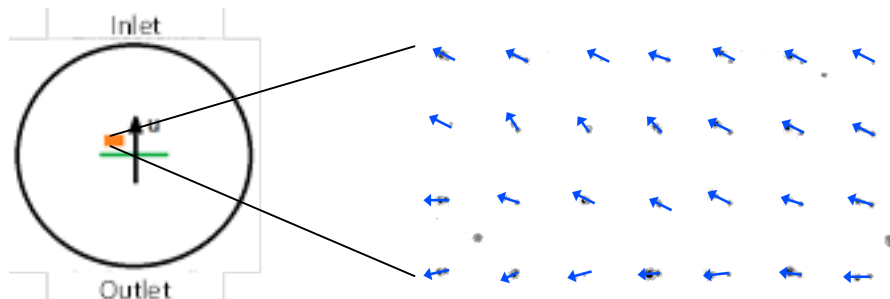


**Fig 7** Deflection of the micro pillars in the array (location is the orange rectangle in the sketch left) in the intake phase at  $47,5^\circ$  CA (original image inverted and with adjusted contrast and brightness, blue arrows indicate deflection). The tumble flow direction along the piston wall is given by the black arrow on the left sketch.

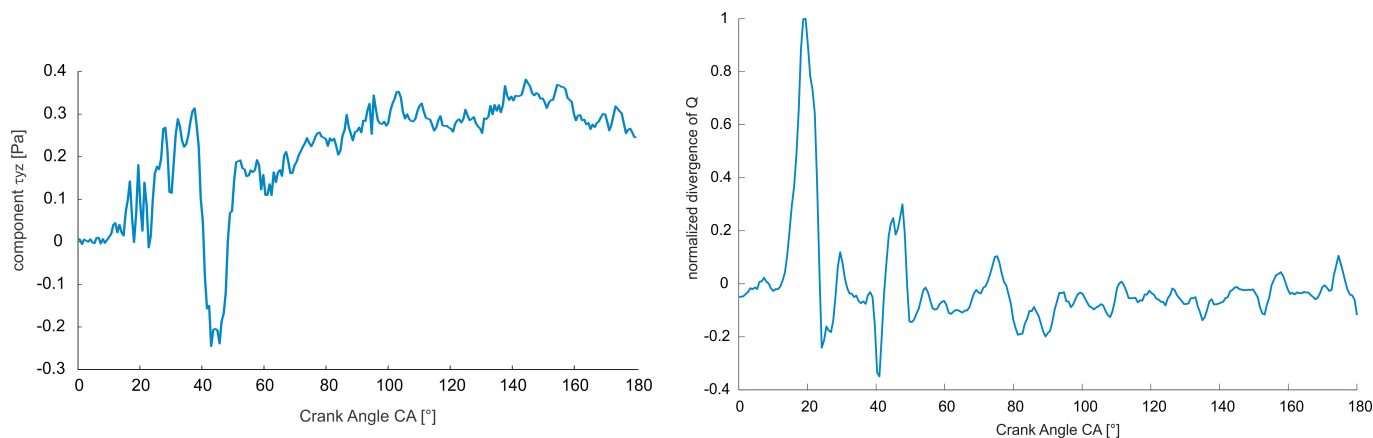


**Fig 8:** Development of the  $yz$ -component of the wall-shear stress over a single intake cycle (original data). On the right, the  $q$ -value at the center of the pillar field.

Fig. 8 shows the sensor signal near the stagnation point which is generated by the jet impacting on the piston wall after opening of the valves. This phase is characterized by larger fluctuations in the WSS. At the same time this interaction generates a first large positive peak in the divergence of the WSS vector field as shown in Fig. 8 at about  $CA=20$ . A positive divergence is caused by flow directed towards the wall while a negative one means fluid motion away from the wall, respectively. Thus, the first positive peak is a footprint of strong flow towards the piston wall by the impacting jet. At later times, the  $q$ -value fluctuates between negative value of -0.3 and positive 0.3 value. A possible explanation is the movement of a vortex along the wall with a down-wash effect at the front and a lift-up at the back. A special event is seen in the sudden reversal of the  $yz$ -component of the WSS value into negative values at  $CA=40^\circ$ . This is accompanied with a shift towards a strong positive divergence. That hints on strong curvature of the flow as reported in earlier measurements using the method of Flying PIV, see Köhler et al. 2015. An example is shown in Fig 9 where the streamline patterns clearly reveal a focus in the center of the location where the pillar field is located. Therefore we assume that a vortex is formed in this region with its axis normal to the wall which generates the so-called tornado effect by interaction of the boundary layer with the vortex core. The radial pressure gradient in the vortex core is imposed on the boundary layer and drives the near-wall fluid, which has lower

momentum than the outer flow towards the center. As a consequence, a strong wall-normal motion is generated at the vortex axis at the wall and fluid is entrained to the center. The combined measurements reveal therefore a clear physical picture of the near-wall flow.

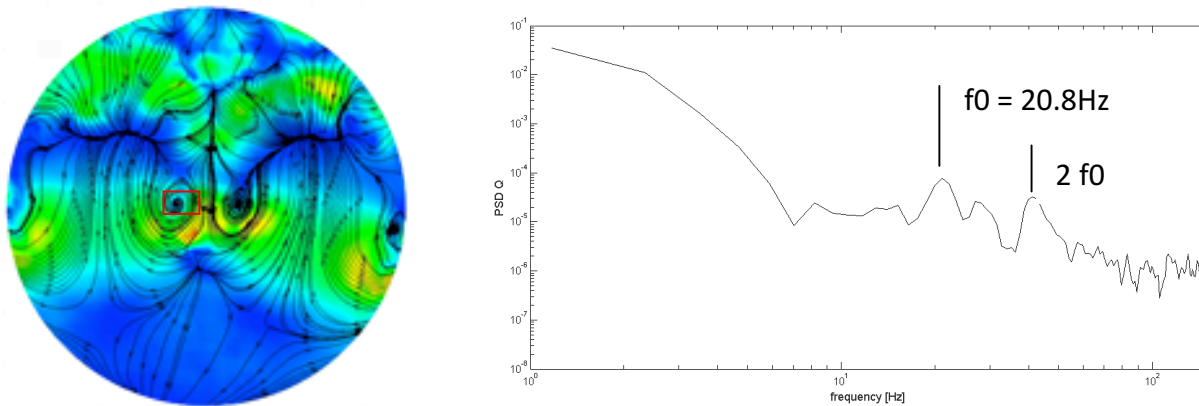


**Fig 9** Left: location of a focus in the measurement region (marked by the red rectangle) measured by Flying PIV; right: spectral distribution of the magnitude of the WSS in the cycle with a primary peak at  $f_0$  and its first harmonic at  $2f_0$ .

For later times  $> CA 80^\circ$  the WSS field gets more homogeneous and flow is dominated by the footprint of the tumble that is forming while divergence is close to zero. So, most of the flow in the investigated region is then parallel to the wall. The WSS reaches values of up to 0.4 Pa in this phase which is comparable to the high WSS at the first phase where the jet is impacting the wall. The waviness in the WSS profile hints on the existence of small scale structures. This is further investigated using spectral analysis of the magnitude of the WSS vector as plotted in Fig 9. A first peak is seen at 20.8 Hz, which first harmonic appears at about 41.3 Hz. The corresponding Strouhal number built with the maximum valve velocity of about 5 times  $U_{max}$  and the valve stroke of 9 mm results in  $St \approx 0.25$ . This corresponds to the shear layer roll-up of the valve jets.

#### 4. Discussion and Conclusion

The present work describes the first application of optical micro-pillar sensors for measuring wall shear stress fields in IC engine flow studies. The proof of the concept to detect the tip deflection of an array of micro-pillars by the sensor through the bottom of the transparent crown has been successfully shown. This is achieved by fluorescent labelling of the micro-pillar tips and the wave-guide properties of the transparent pillars. The measurements document the different

phases of the near-wall flow, the first one is dominated by the impact of the jets generated at the valve with the piston crown. This phase is characterized by small scale structures and high-frequency fluctuations in the WSS profile driven by the jet shear layer instabilities at jet Strouhal numbers estimated to  $St \approx 0.25$ . Later on the flow homogenizes and orients into direction of the tumble flow near the wall. Peak WSS values are about 0.4 Pa and are similar to the first phase. Using more compact and more powerful cameras will pave the way to maximize the imaging area without loss of resolution, thus recording larger areas of the micro-pillar fields.

### Acknowledgment

Part of the project was funded by the Air Force Office of Scientific Research, Air Force Material Command, USAF under Award No. FA9550-14-1-0315 and program manager Russel Cummings. Funding of the position of Professor Christoph Brücker as the BAE SYSTEMS Sir Richard Olver Chair in Aeronautical Engineering is gratefully acknowledged herein.

### References

- Borée J., Miles P. C. (2014) In-Cylinder Flow. Encyclopedia of Automotive Engineering, Online 2014 John Wiley & Sons, Ltd. DOI: 10.1002/9781118354179
- Brücker C, Spatz J, Schroeder W (2005) Feasibility study of wall shear stress imaging using micro-structured surfaces with flexible micro-pillars *Exp. Fluids* **39** 464–474
- Brücker C, Bauer D, Chaves H (2007) Dynamic response of micro-pillar sensors measuring fluctuating wall-shear-stress *Exp. Fluids* **42** 737–749
- Brücker C (2015) Evidence of rare backflow and skin-friction critical points in near-wall turbulence using micropillar imaging *Phys Fluids* **27**, 031705
- Hasse C, Sohm V, Durst B (2010) Numerical investigation of cyclic variations in gasoline engines using a hybrid URANS/LES modelling approach. *Computers & Fluids* **39** 25–48
- Koehler M, Hess D, Brücker C (2015) Flying PIV measurements in a 4-valve IC engine water analogue to characterize the near-wall flow evolution, *Meas. Sci. Technol.* **26** (2015) 125302 (9pp)
- Skupsch C, Klotz T, Chaves H, Brücker C (2012) Channeling optics for high quality imaging of sensory hair, *Rev Sci Instrum* **83** 045001
- Voisine M, Thomas L, Borée J, Rey P (2011) Spatio-temporal structure and cycle to cycle variations of an in-cylinder tumbling flow. *Exp Fluids* **50**:1393-1407